International Journal of Bridge Engineering (IJBE), Special Issue 2017, pp. 25-52

PRECAST PIERS WITH GROUTED SPLICE SLEEVE CONNECTIONS FOR ACCELERATED BRIDGE CONSTRUCTION IN SEISMIC ZONES

M. J. Ameli[1] , Chris P. Pantelides[2]

[1]Graduate Engineer, Walter P. Moore, Diagnostics Group, Houston, TX, USA
[2]Professor, Dept. Civil and Environmental Engineering, Univ. of Utah, Salt Lake City, UT, USA
e-mail: mameli@walterpmoore.com, c.pantelides@utah.edu

ABSTRACT: The grouted splice sleeve (GSS) connection has been frequently used in non-seismic regions because it offers ease and acceleration of overall construction. In seismic regions, research studies are still in progress to assess the application of GSS connections as part of the accelerated bridge construction (ABC) initiative. In this study, a summary of experimental results is provided from half-scale experiments of ABC columns under cyclic quasi-static loading, addressing performance differences between GSS and cast-in-place monolithic connections. A modeling strategy is described for precast single-column bridge piers with GSS connections. Prototype precast bridge pier models are created using the proposed strategy for GSS connectors inside the column with debonded bars in the footing. The bridge pier models are examined using nonlinear static cyclic analysis to obtain the capacity. Parametric studies are performed for both the cast-in-place and precast single-column bridge piers to investigate the influence of column height, longitudinal steel ratio, axial load, plastic hinge length, displacement ductility, curvature ductility, and amount of transverse reinforcement. The global strength of cast-in-place and precast column models was found to be similar. For the precast alternatives bar fracture occurred in fewer cycles, ultimate displacement was comparable and displacement ductility was smaller than the cast-in-lace models.

KEYWORDS: Accelerated bridge construction; Computational study; Grouted splice sleeve; Mechanical coupler; Precast concrete.

1 INTRODUCTION

Accelerated bridge construction (ABC) offers speed, safety, improved quality, and reduced environmental impact in bridge construction. Precast concrete components are frequently used as part of ABC. The focus of this paper is the design of moment-resisting connections for bridge substructures in moderate-to-high seismic zones using precast components. Connections of precast substructure components include the socket connection between column and footing [1-5], the grouted duct connection between column and footing or cap

beam [6-8], and the grouted splice sleeve (GSS) connection [9-21]. In this paper, a parametric study is conducted to ascertain the response sensitivity of a computational model to varying parameters [22]. A summary of experimental results is provided from half-scale experiments of ABC columns under cyclic quasi-static loading, with an emphasis on performance differences between GSS connections and cast-in-place monolithic connections. A monolithic and a precast single-column pier with similar configurations were examined with two different levels of longitudinal reinforcement ratio, column height, axial load, and displacement ductility capacity. Overall, 32 columns were investigated and results are discussed in terms of strength, displacement capacity, global response, and local response; moreover, seismic performance comparisons are made between the monolithic and precast alternatives.

2 SUMMARY OF EXPERIMENTS

An experimental program for cyclic testing of column-footing connections has been completed [21]. As part of this program, three half-scale concrete specimens are described, two of which were constructed using precast concrete components joined by means of GSS connectors, as shown in Figure 1. The dimensions of the column and footing are shown in Figure 1a. The control specimen (CIP) was constructed monolithically without any GSS connectors (Figure 1b). The connectors were incorporated in the footing of specimen Precast-1, with dowel bars extending from the column end (Figure 1c). The second precast specimen, Precast-2, had a footing connected to a column using GSS connectors cast in the column base; dowel reinforcing bars extended from the footing that were debonded from concrete over a length of 203 mm just below the footing-to-column interface (Figure 1d).

2.1 Specimen design

The specimens were designed according to the AASHTO Guide Specifications for LRFD Seismic Bridge Design [23], the AASHTO LRFD Bridge Design Specifications [24], and the Caltrans Seismic Design Criteria [25]. For bridges located in moderate-to-high seismic areas these design codes prohibit splicing of reinforcement, including mechanical splicing devices, in the plastic hinge region of ductile members; for the AASHTO Guide Specifications this applies to Seismic Design Categories C and D. The initial design was developed for a cast-in-place condition without any GSS connectors, i.e. specimen CIP. The design was then modified for GSS connectors within the precast subassemblies. The column height was 2.59 m with a 533-mm octagonal cross-section. Column reinforcement consisted of six 25M bars in a circular arrangement and a 13M spiral with a 64 mm pitch. The desirable column failure mode was either flexural or splice failure. Longitudinal and transverse reinforcement ratios were

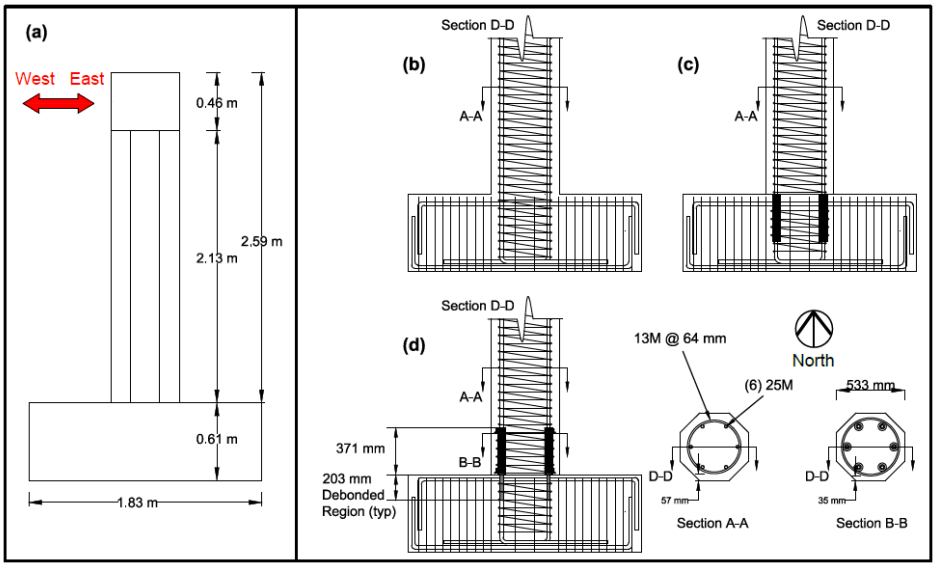

Figure 1. Specimen details: (a) Subassembly dimensions, (b) CIP, (c) Precast-1, and (d) Precast-2

1.3% and 1.9%, respectively. The precast concrete footing was designed to remain elastic with dimensions of 1.83-m long by 0.91-m wide by 0.61-m deep and was reinforced with 25M longitudinal bars enclosed by 13M double hoops. The specimens were tested under quasi-static cyclic loads applied at the 0.46-m deep column stub as shown in Figure 1a.

2.2 Experimental performance

The response of the specimens is shown in terms of hysteresis loops and the extent of the damaged zone (Figure 2). Damage states included: flexural cracks and concrete cover spalling (indicating end of cracking stage, which coincided with initiation of cover concrete spalling), yield penetration (referring to localized damage around reinforcing bars at the column-to-footing interface resulting from yielding of the column bars and penetrating deeper into the footing), and fracture of column longitudinal bars (due to low-cycle fatigue for all test subassemblies). Control specimen CIP had stable hysteresis loops with spalling of the unconfined concrete cover. The extreme west column reinforcing bar of CIP fractured at the end of the second cycle of the 8% drift ratio, at a section 38 mm above the column-footing interface, which was followed by fracture of the extreme east column reinforcing bar during the first cycle of the 9% drift ratio, 51 mm above the interface due to low-cycle fatigue. The specimen achieved a displacement ductility of 8.9. Spalling of concrete was observed in the plastic hinge region, in addition to the fractured column bar and exposed spiral as shown in Figure 2a.

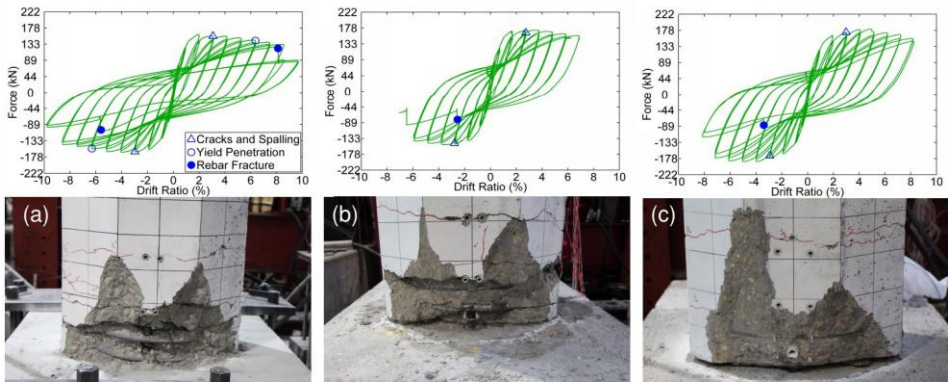

Figure 2. Hysteresis curves and final damage of specimens: (a) CIP, (b) Precast-1, and (c) Precast-2

Specimen Precast-1 had stable performance up to the 7% drift ratio, during which the extreme east column reinforcing bar fractured at a section 51 mm above the column-footing interface, due to low-cycle fatigue. The displacement ductility of this specimen was found to be equal to 6.1. A damage state similar to that of CIP was observed, with spalled concrete, flexural cracks, and exposed spiral (Figure 2b). The hysteretic curves of specimen Precast-2 showed a ductile performance. The hysteresis loops were wide and stable with minimal strength deterioration up to the first cycle of the 8% drift ratio, when the extreme east column reinforcing bar fractured 13 mm below the column-footing interface due to low-cycle fatigue. Debonding of dowel bars inside the footing resulted in better performance compared to Precast-1. The displacement ductility of this specimen was 6.8. Fewer flexural cracks and concrete spalling with a smaller depth was observed, as shown in Figure 2c.

With respect to the hysteretic response of Specimen CIP the precast subassemblies had a comparable strength but lower displacement capacity. This is attributed to combination effects resulting from the pre-existing separation joint at the interface of the column and footing, along with the presence of the GSS connectors adjacent to the interface.

3 MODELING STRATEGY

In moderate-to-high seismic regions, the connections between prefabricated elements are critical for adequate performance, especially if GSS connectors are used at moment-resisting joints. A reliable modeling strategy which is able to predict the seismic response of precast bridge columns with GSS connectors is needed for design of these elements.

3.1 Computational model for experimental specimens

As a first step in developing a robust and simple design procedure for

prefabricated column-footing connections using GSS, a seismic analysis method was developed which is described in detail elsewhere [22]. The analysis method was calibrated with the column-footing connection experimental results presented in Section 2.2. A two-dimensional computational model was developed for seismic analysis of precast bridge columns connected with grouted splice sleeve connectors. The modeling strategy is based on transformation of the model for the precast column with GSS connectors, to an idealized equivalent cast-in-place column with a reduced plastic hinge length that is capable of simulating both global and local response.

A force-based beam-column element type with plastic hinge integration scheme [26] was used in an iterative procedure to determine the unique reduced plastic hinge length of the equivalent cast-in-place column and reproduce the experimental results. The model includes bond-slip of reinforcing bars in addition to low-cycle fatigue and was successful in replicating both global and local responses. The low-cycle fatigue bar fracture was accounted for using a reinforcing steel material capable of predicting the low-cycle fatigue life of steel bars, which was validated with a comprehensive test series on steel bars under high strain reversal protocols [27]. Based on such a model, low-cycle fatigue life of a reinforcing bar is reduced with an increase in plastic strain imposed on the bar. According to the test results, a premature bar fracture occurred for the precast subassemblies due to a higher strain demand on the column bars at the interface between the column and footing.

The plastic hinge length of the validated computational model for the CIP specimen was in good agreement with available empirical relationships, while a reduced plastic hinge length equal to 4/6 and 5/6 times the CIP plastic hinge length was obtained for the idealized equivalent model of Precast-1 and Precast-2, respectively. The reduced plastic hinge length was found to be 0.38 and 0.48 times the cross-sectional dimension of the column for Precast-1 and Precast-2, respectively.

The proposed model was developed as a simplified approach towards simulating the relatively complex behavior of precast columns with GSS connectors. Even though the bond-slip parameters, i.e. grout strength and reinforcing bar embedment depth, along with geometric parameters of the column were explicitly included in obtaining the plastic hinge reduction factors for the precast column models. More experiments are needed to implicitly include the referenced parameter in developing a relationship for the plastic hinge length of precast columns with GSS connectors.

3.2 Modeling strategy for single column piers

The implementation of a plastic hinge modeling strategy offers a simplified approach for seismic design of flexural precast concrete columns with GSS connectors. However, this implementation requires a comprehensive study of

the response sensitivity of the model to potential changes in pertinent modeling parameters. For conventional bridges with modern seismic detailing, the most important column parameters include longitudinal reinforcement ratio, column aspect ratio, axial load, and design displacement ductility.

The selection of the above-mentioned parameters was based on their effect on the response of a ductile bridge column as per current state of practice, in accordance with capacity design procedures. The aspect ratio of the column is an important property that can change the bond-slip dominated response into a flexural dominated response, which plays an important role for a precast column. The axial load applied to the column can change the strain demand on reinforcing bars within the plastic hinge and ultimately affect the failure point of the column due to low-cycle fatigue. The reinforcing bar ratio is an important parameter with respect to strength properties of the column, whereas, design displacement ductility is a key parameter in determining the displacement properties of such columns.

A parametric study was developed by considering two different values associated with each of the aforementioned four parameters, using a 914-mm circular column reinforced with 29M longitudinal bars. Two levels of longitudinal reinforcement ratio were selected considering practical aspects of the design, that is, 1.38% and 1.96% corresponding to fourteen 29M and twenty 29M bars, respectively. Two column aspect ratios equal to 4.0 and 5.0 were included indicating a column clear height of 3.66 m and 4.57 m, respectively. Two axial load levels were employed with an axial load index (ALI) equal to 5% and 10%. Lastly, design displacement ductility values equal to 7.0 and 11.0 were considered to study different transverse reinforcement alternatives. The AASHTO Guide Specifications [23] and the Caltrans Seismic Design Criteria [25] limit the design displacement ductility to 6 and 5 to account for practical design aspects, by reducing the amount of transverse reinforcement required to obtain a certain confinement level; and, most importantly, to limit the probable damage to the column as a result of a design level event. The design displacement ductility of 11.0 used in this study was used only to investigate the possibility of obtaining such a highly ductile response based on the available design approaches.

The parametric study was carried out for columns with details similar to CIP, i.e., monolithic construction with no GSS connectors, and for columns with details similar to Precast-2 which had GSS connectors in the column and debonding of footing bars for a length equal to 8.0 times the bar the diameter within the footing.

4 PARAMETRIC STUDY

Sixteen CIP column models in addition to sixteen Precast-2 column models were studied using OpenSees, to investigate the response of the proposed

modeling strategy to varying parameters. The columns for the two alternatives were assumed to represent bridge piers from a single-column bent with a cantilever configuration (Figure 3). The footing is assumed to be a 2.13-m long by 2.13-m wide by 0.91-m deep capacity protected member with adequate reinforcement to resist the load effects transferred from the column.

4.1 Design procedure

The 32 modeling cases considered in this study are shown in Table 1, which highlights the major differences between the alternatives. The alternatives were grouped in pairs with corresponding details for the models representing CIP and Precast-2 type columns as discussed in Section 2. The transverse reinforcement which was composed of closed circular single or double hoops was designed for a required level of confinement. This is the critical variable for the design displacement ductility values equal to 7.0 and 11.0; shear reinforcement does not govern the design for such slender and ductile columns. Details of the transverse reinforcement can be found in Section 5.

A series of sectional analyses were carried out to determine the size and number of hoops required to achieve a certain level of displacement ductility. The displacement ductility capacity (μ_D) of a cantilever column, curvature ductility (μ_φ) of the corresponding section, length of the plastic hinge (L_p), and height of the column (H) are related through the following equation [28]:

$$\mu_D = 1 + 3(\mu_\phi - 1)\frac{L_p}{H}\left(1 - 0.5\frac{L_p}{H}\right) \quad (1)$$

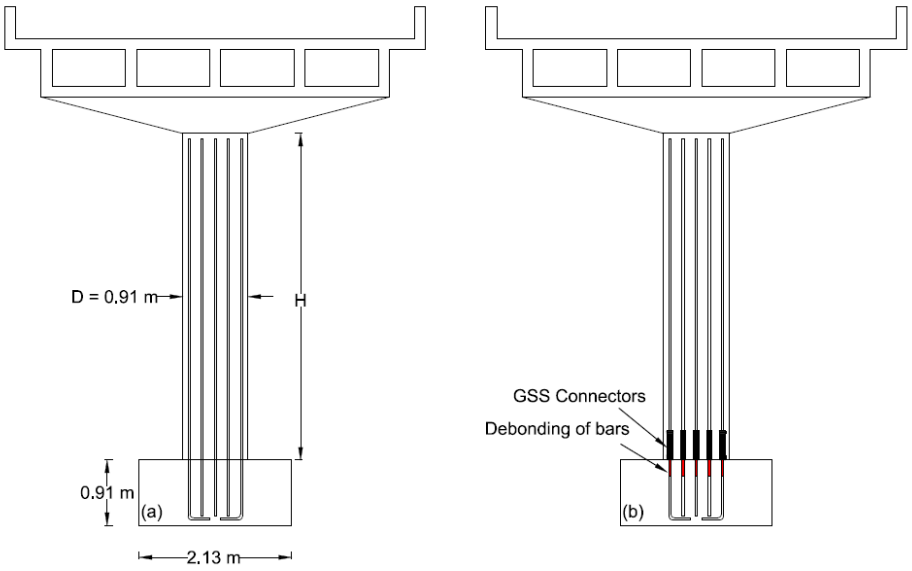

Figure 3. Schematic of the two model types: (a) CIP; (b) Precast-2

By rearranging Eq. (1) curvature ductility is defined as a function of the given displacement ductility, as shown in Eq. (2):

$$\mu_\phi = \frac{\mu_D - 1 + 3\frac{L_p}{H}(1 - 0.5\frac{L_p}{H})}{3\frac{L_p}{H}(1 - 0.5\frac{L_p}{H})} \quad (2)$$

The plastic hinge length is obtained from a relationship which gives good agreement with the experiments conducted in this research [29]; actual displacement capacity of the tested CIP column was smaller than the calculated value using the plastic hinge length relationship in [28], because a different failure mode of bar fracture due to low-cycle fatigue occurred before hoop fracture, or core concrete crushing. The plastic hinge length is given as [29]:

$$L_p = 0.12L_s + 0.014\alpha_{sl} d_b f_y \quad (3)$$

where L_s is the shear span which in this case is equal to H, a_{sl} is equal to 0.0 if bar pullout is not present and is equal to 1.0 if pullout is present, d_b is the diameter of the column longitudinal bar (m), and f_y is the bar yield strength in MPa. Parameter a_{sl} was assumed zero for validation of the modeling strategy since no pullout of column bar with GSS connectors was observed in the experiments; hence, it was assumed that a_{sl} was zero for the models used in this research, knowing that modern seismic design procedures would prevent anchorage issues and pullout failure. As a result, Eq. (2) can be simplified further and be presented as a function of the required displacement ductility capacity, as shown in Eq. (4).

$$\mu_\phi = 2.96\mu_D - 1.96 \quad (4)$$

When the required curvature ductility is known, a moment-curvature analysis is carried out using a trial transverse reinforcement scheme. Subsequently, an idealized moment-curvature curve is constructed to obtain the curvature ductility for the assumed column section. The idealized moment-curvature curve consists of: (1) a sloped line that intersects the actual curve at a point where the extreme reinforcing bar yields; (2) a horizontal line connecting the effective yield point and the ultimate point of the section. The ultimate point corresponds to onset of confined core crushing; the effective yield point is found by balancing the areas under the actual and idealized curves. If the obtained curvature ductility was equal to or larger than the required value, the design was accepted, otherwise more trials were performed.

An expected concrete compressive strength (f'_{ce}) equal to 41.4 MPa was used for the unconfined concrete along with an ultimate unconfined strain (ε_{cu}) equal to 0.005. Properties for confined concrete were found using Mander's model [30]. Concrete04 from the OpenSees material library [31] was used for both

Table 1. Modeling alternatives for parametric study

Model No.	Details	Bar Ratio (%)	Column Aspect Ratio	ALI (%)	Displacement Ductility*
1	CIP	1.38	4	5	7.0
2	Precast-2	1.38	4	5	6.1
3	CIP	1.38	4	5	11.0
4	Precast-2	1.38	4	5	9.4
5	CIP	1.38	4	10	7.0
6	Precast-2	1.38	4	10	6.1
7	CIP	1.38	4	10	11.0
8	Precast-2	1.38	4	10	9.4
9	CIP	1.38	5	5	7.0
10	Precast-2	1.38	5	5	6.1
11	CIP	1.38	5	5	11.0
12	Precast-2	1.38	5	5	9.4
13	CIP	1.38	5	10	7.0
14	Precast-2	1.38	5	10	6.1
15	CIP	1.38	5	10	11.0
16	Precast-2	1.38	5	10	9.4
17	CIP	1.96	4	5	7.0
18	Precast-2	1.96	4	5	6.1
19	CIP	1.96	4	5	11.0
20	Precast-2	1.96	4	5	9.4
21	CIP	1.96	4	10	7.0
22	Precast-2	1.96	4	10	6.1
23	CIP	1.96	4	10	11.0
24	Precast-2	1.96	4	10	9.4
25	CIP	1.96	5	5	7.0
26	Precast-2	1.96	5	5	6.1
27	CIP	1.96	5	5	11.0
28	Precast-2	1.96	5	5	9.4
29	CIP	1.96	5	10	7.0
30	Precast-2	1.96	5	10	6.1
31	CIP	1.96	5	10	11.0
32	Precast-2	1.96	5	10	9.4

* Assuming identical confinement level is to be provided for CIP and precast alternatives for comparison.

unconfined cover concrete and confined core concrete. ReinforcingSteel from the OpenSees material library was assigned to the column reinforcing bars. Table 2 includes properties for the Grade 414 MPa ASTM A706 29M reinforcing bars used in this study which conform to AASHTO Guide Specifications [23].

Based on findings of the experimental study, reduced displacement capacity of precast specimens was simulated by incorporating a reduced plastic hinge length [22]. The reduction factor previously determined for the reduced plastic hinge length of specimen Precast-2 was applied to the precast alternatives for the parametric study as:

$$L_{p,GSS} = \gamma_{GSS} L_p \tag{5}$$

where, $L_{p,GSS}$ is the reduced plastic hinge length of a precast column with GSS connectors in the column end and debonding of footing dowels for a length 8.0 times the bar diameter, and γ_{GSS} is a reduction factor for columns with such details; this was found to be equal to 5/6 as noted in Section 3.1.

A one-dimensional bond-slip model was used to obtain the pseudo stress-strain relationship for reinforcing bars inside the plastic hinge region, which includes softening effects from bond-slip [22]. The end displacement of a 29M bar embedded in conventional concrete was obtained for each modeling alternative with a different column height and was divided by the corresponding plastic hinge length to find the pseudo strain. The bond-slip idealization for models of precast columns was composed of a 29M factory dowel and a 29M field dowel grouted inside a 29M GSS, in addition to the debonded bar segment which was an extension of the field dowel. The grout strength was assumed as 100 MPa. Confined and unconfined bond constitutive laws were used; unconfined properties were employed over unconfined areas near the two openings, referred to as the cone depth. The cone depth was obtained assuming a cone angle of 45^0 which resulted in 11 mm and 4 mm for the field and factory dowel, respectively. The total embedded length was taken as 200 mm and 192 mm for the field and factory dowel, respectively.

4.2 Details of model alternatives and model layout

Examples of typical computational models with the details of the 4.57-m high column reinforced with fourteen 29M longitudinal bars are shown in Figure 4.

Table 2. Reinforcing bar material properties

Quantity	Value
Specified Yield Stress, f_y	414 MPa
Expected Yield Stress, f_{ye}	469 MPa
Expected Tensile Strength, f_{ue}	655 MPa
Strain at Onset of Strain Hardening, ε_{sh}	1.25%
Reduced Ultimate Tensile Strain, ε^R_{su}	9.00%
Ultimate Tensile Strain, ε_{su}	12.00%

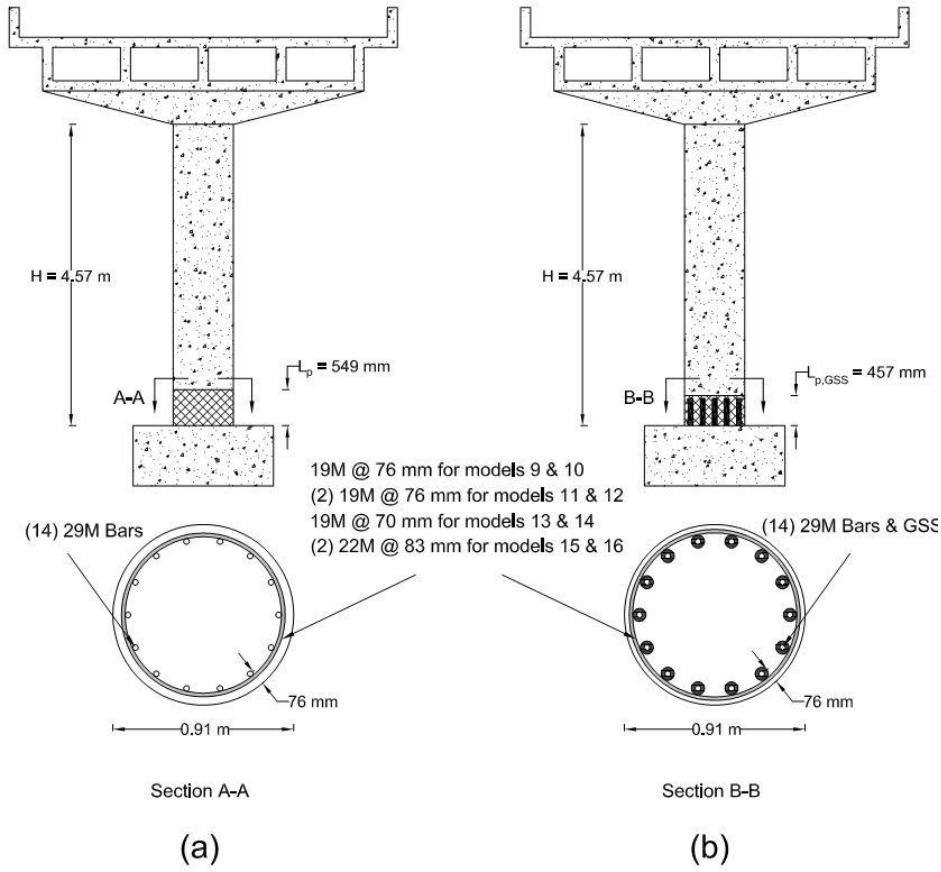

Figure 4. Details of column models with H = 4.57 m and (14) 29M bars: (a) CIP; (b) Precast-2

The plastic hinge length for the CIP and Precast-2 models was 549 mm and 457 mm, respectively.

The layout for the cantilever column models is composed of two end nodes connected by a nonlinear beam-column element with a plastic hinge integration scheme [26], as shown in the overall layout of the proposed model in Figure 5. The axial load was applied at the top node, before the static cyclic displacement was applied, using a displacement history similar to the one used in the experiments composed of two cycles per drift ratio with increasing amplitude. The orientation of the model indicates that the analysis is carried out in the transverse direction of the bridge with the columns in single-curvature configuration. A shorter plastic hinge length was used for the Precast-2 model compared to the CIP model, as shown in Eq. (5). The column sectional arrangements with the given details are different for regions inside and outside the plastic hinge length as shown in Figure 5. Envelopes for the uniaxial

materials assigned to each fiber are also shown (Figure 6). Mander's model [30] was used to obtain the properties of the confined concrete. Concrete04 material was used for both confined and unconfined concrete. ReinforcingSteel material was assigned to steel fibers inside and outside the plastic hinge region; however, as discussed in [22], a pseudo stress-strain behavior was used inside the plastic hinge region to account for the softening effects of bond-slip. ReinforcingSteel with conventional steel properties (Table 2) was incorporated for column longitudinal bars outside the plastic hinge region. The expected material properties were used in this study.

5 COMPUTATIONAL RESULTS

The analysis termination criterion, which represents the failure point for each column model, was set to be either crushing of extreme core concrete fiber or fracture of column longitudinal bars as a result of low-cycle fatigue. The hysteresis response of column model 1 and model 2 alternatives is shown in Figure 7; bar fracture due to low-cycle fatigue is identified for both models. For model 1 with CIP details, two column bars fractured during the first cycle of the 7% drift ratio, while four column bars fractured during the second cycle of the 7% drift ratio. For model 2 with Precast-2 details, two column bars fractured during the second cycle of the 6% drift ratio. This implies that the precast model

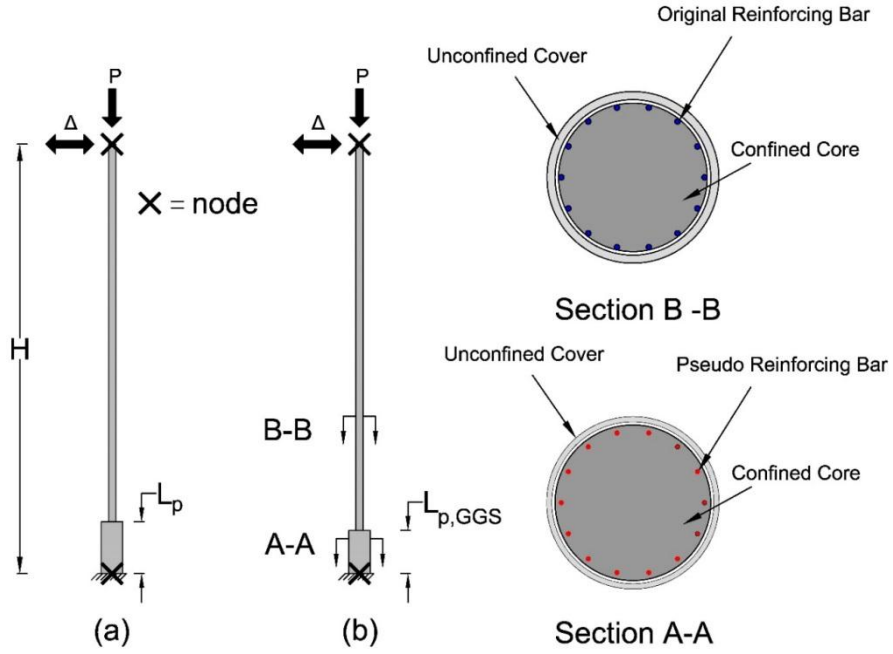

Figure 5. Example of column model layout: (a) column model 9 (CIP); (b) column model 10 (Precast-2)

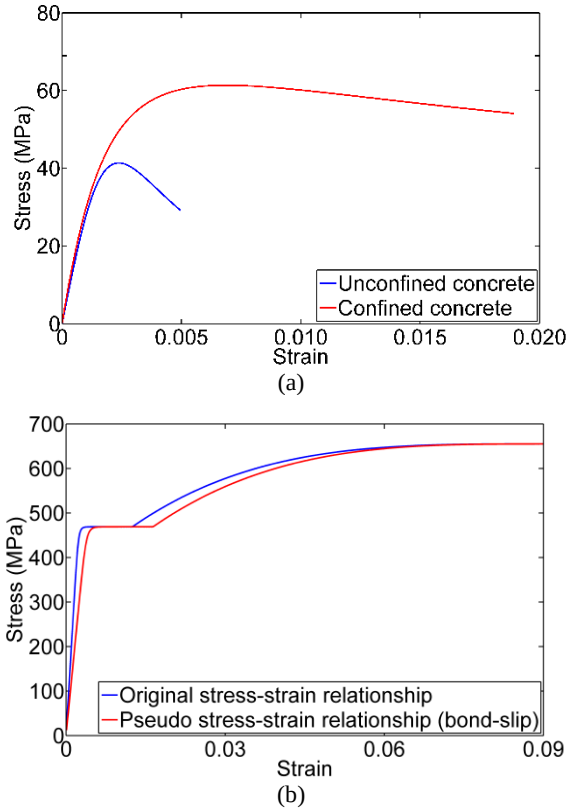

Figure 6. Uniaxial material properties for column model 10: (a) concrete (CIP); (b) reinforcing bar

had premature bar fracture due to simulated localized demand because of a reduced plastic hinge length; hence, the failure mode was low-cycle fatigue fracture of column bars. The ultimate drift was equal to 6% or 220 mm of displacement for both columns. However, this was not always the case; for example column model 6 with Precast-2 details failed due to crushing of core concrete at the peak displacement of the first cycle during the 6% drift ratio. The ultimate displacement for column model 6 was equal to 194 mm corresponding to a 5.3% drift ratio.

5.1 Comparison of CIP and Precast-2 design alternatives

The major difference between CIP and Precast-2 alternatives is the plastic hinge length. The integration weight associated with each integration point along the column changes by specifying a new plastic hinge length for the precast model. This mainly affects the integration point at the column end which, for the

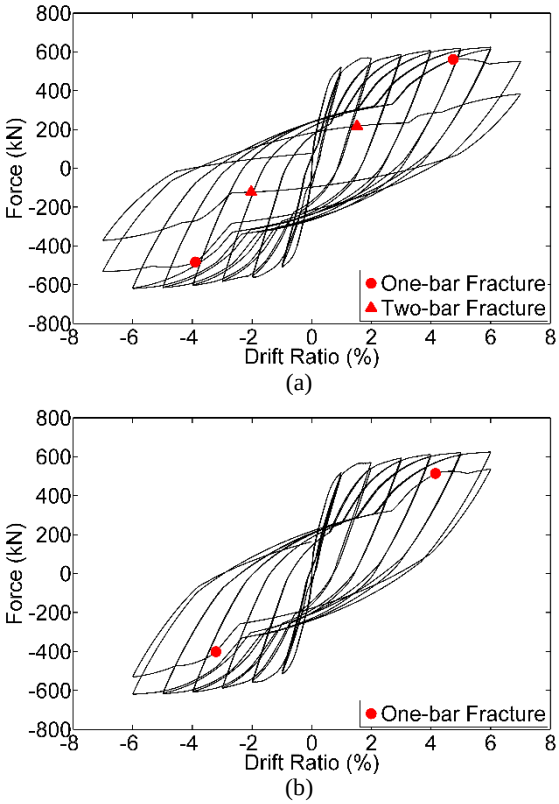

Figure 7. Example of hysteresis response: (a) column model 1 (CIP details), ultimate drift = 6.0%; (b) column model 2 (Precast-2 details), ultimate drift = 6.0%

particular case of a cantilever column, is the most effective integration point.

A representative comparison of model responses is provided in terms of both global and local response. A complete list of comparisons is provided elsewhere [32]. The cyclic envelope of the hysteresis response is presented along with the strain variation in an extreme column longitudinal bar. The displacement ductility capacity (μ_C) is obtained using an approach similar to that for determining curvature ductility. The failure mode is discussed in addition to the peak compressive strain at the extreme fiber of the core concrete.

Column models 1 and 2 were 3.66-m high reinforced with fourteen 29M main bars and 19M closed hoops at 76 mm on center. An axial load equal to 1358 kN was applied to these models. The global response represented by the cyclic envelope indicates that there was a minimal difference between the two alternatives as shown in Figure 8. There was a 12% reduction in the initial elastic slope of the precast model due to a pronounced bond-slip. The strain variation in the extreme longitudinal bar implies that a larger demand was introduced to the

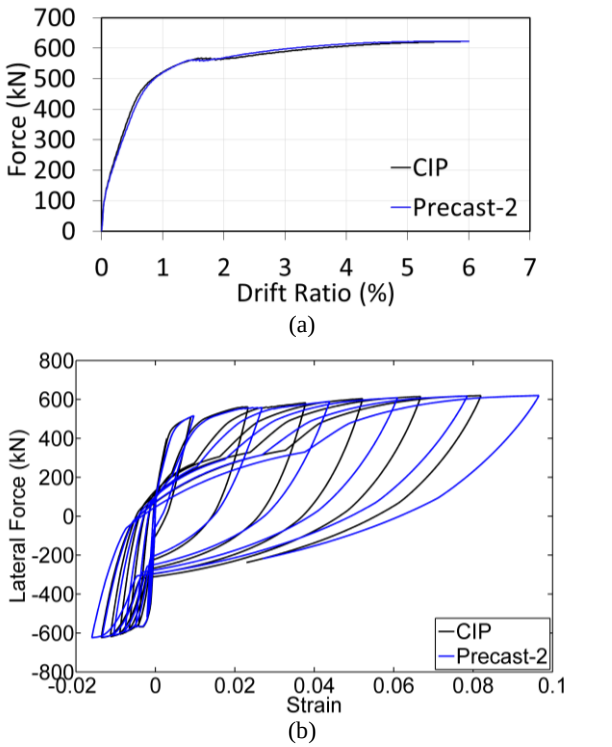

Figure 8. Comparison of column model 1 (CIP) and 2 (Precast-2): (a) cyclic envelope; (b) strains in the column extreme bar

column end of the precast alternative which resulted in premature fracture of column bars. As discussed in Section 5, column bar fracture occurred during the first and second cycle of the 7% drift ratio for CIP, whereas bar fracture occurred during the second cycle of the 6% drift ratio for Precast-2. At the peak displacement during the 7% drift ratio, the compressive strain in the extreme fiber of the core concrete was 1.71% and 1.90% for CIP and Precast-2, respectively. Compared to the strain at onset of core crushing for these two models, $\varepsilon_{cu} = 1.90\%$, it is observed that there was a margin of 9.8% before the core crushed for CIP, while the core compressive strain was equal to the ultimate strain for Precast-2 implying that the compressive strains were 10.8% larger than the CIP model.

The failure mode of both column models 1 and 2 was found to be bar fracture due to low-cycle fatigue. Therefore, the ultimate displacement was associated with the peak displacement of the cycle prior to occurrence of bar fracture. This was found to be 220 mm, which is 6% in terms of drift ratio. The displacement ductility capacity was equal to 6.82 for CIP, and 6.13 for Precast-2. The cyclic envelope along with the idealized curve constructed to obtain the displacement ductility values is shown in Figure 9.

5.2 Effect of various parameters on the response of the column models

Four parameters were influential in the analysis of the 32 alternative models; these are design displacement ductility, column axial load, column height, and number of column longitudinal bars. The cyclic envelopes for all CIP models reinforced with fourteen 29M longitudinal bars was determined as shown in Figure 10a. The overall response of the columns follows expected behavior of reinforced concrete members under simultaneous lateral and axial loading. Strength capacity of the columns increased with increasing axial load, whereas it decreased with increasing column height. Similarly, the columns with twenty 29M longitudinal bars had expected performance under the varied parameters. The cyclic envelopes for eight CIP alternatives with twenty 29M longitudinal bars are shown in Figure 10b. For brevity, effects of parameter variation are only discussed using CIP columns, since it was observed that the precast alternatives had a similar global response to the corresponding CIP columns, while an increased sectional deformation was achieved representing a more localized demand. For the precast columns, the response trend was the same as in CIP alternatives under changing parameters. Table 3 lists displacement ductility capacity values for all 32 column models. All precast columns had a smaller displacement ductility capacity compared to CIP columns. The displacement ductility capacity values were always smaller than the required values for both CIP and Precast-2 models.

The difference between required and obtained values was more pronounced for columns with a design displacement ductility capacity equal to 11.0. The reason is that the termination criterion used in the design displacement ductility procedure was based on the onset of core concrete crushing; analysis results showed that low-cycle fatigue bar fracture occurred prior to core concrete crushing for 29 of the 32 models. Low-cycle fatigue bar fracture is highly sensitive to characteristics of the loading history and resulting strain history for individual longitudinal column bars. The findings of this paper apply to the specific loading history developed based on extensive research for reinforced concrete components [33].

Precast column model 22 had the lowest displacement ductility capacity of $\mu_C = 5.57$ among all column models. This was attributed to a relatively large axial load applied to this column which had a shorter analytical plastic hinge compared to its CIP alternative; as a result, concrete core crushing occurred before bar fracture. The results suggest that there is an upper bound displacement ductility capacity due to low-cycle fatigue bar fracture which is likely to occur under ground motions with many large-amplitude cycles. For instance, a

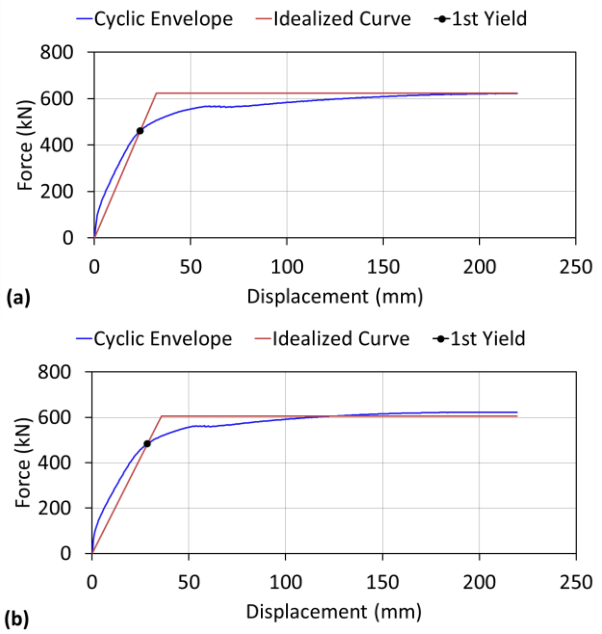

Figure 9. Displacement ductility capacity: (a) column model 1 (CIP), $\mu_C = 6.82$; (b) column model 2 (Precast-2), $\mu_C = 6.13$

displacement ductility capacity of 11.0 is not achievable for bridge columns with details similar to the columns studied herein. The following sections provide a more detailed discussion on the effect of each parameter on the response of the column models.

5.3 Effect of design displacement ductility

Two different design displacement ductility values equal to 7.0 and 11.0 were studied. The conventional design procedure outlined in bridge code specifications takes into account core crushing, or hoop fracture, when obtaining the design displacement ductility. However, it was noted that for the specific column configurations considered herein, a different failure mode was achieved for all columns, which is low-cycle fatigue bar fracture. Therefore, regardless of the design objective, most of the columns only performed up to a 7% and 8% drift ratio for the 3.66-m and 4.57-m high columns, respectively.

The cyclic envelopes of models 1 and 3 with design displacement ductility equal to 7.0 and 11.0, respectively, are shown in Figure 11a. It is observed that both columns had a similar initial and post-cracking stiffness. The post-yield strength of column model 3 was slightly larger than that of model 1 which is due to a stronger core concrete as a result of better confinement. The ultimate displacement capacity was identical as both columns failed during the same cycle and drift ratio because

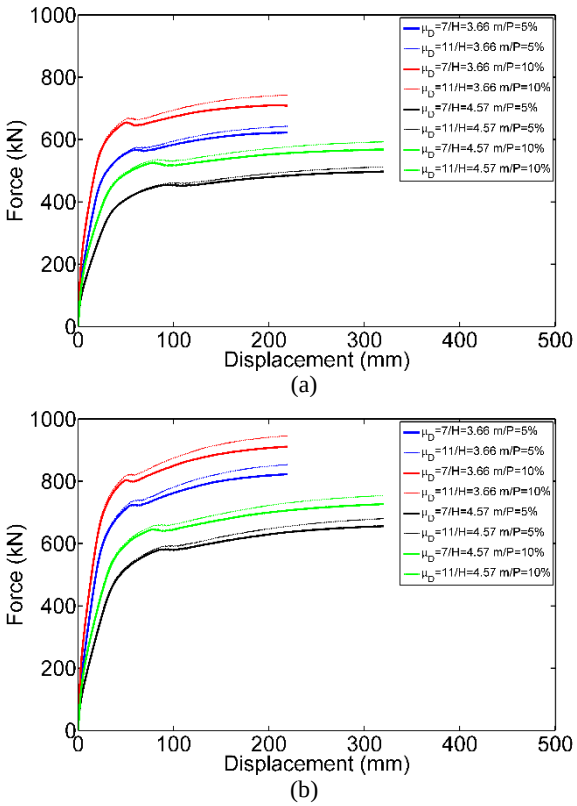

Figure 10. Comparison of global column response: (a) reinforced with (14) 29M bars; (b) reinforced with (20) 29M bars

of low-cycle fatigue bar fracture. The strain variation for an extreme column bar of both columns (Figure 11b) indicates that the difference between the columns was insignificant. The tensile strains were slightly larger while compressive strains were slightly smaller for model 3. This is attributed to a stronger core concrete which resulted in a reduction of the section's neutral axis depth.

5.4 Effect of axial load

Axial loads of 1358 kN and 2716 kN were employed which corresponds to a 5% and 10% ALI, respectively, to study the global and local response of the models. In general, for columns with relatively low axial load, such as bridge columns, the lateral force capacity increases with an increase in axial load as long as the sectional demand remains below the balanced point of sectional capacity. This behavior is observed as shown in Figure 12a, which shows the cyclic envelopes for model 1 and model 5 under 5% and 10% axial load, respectively. There was a 14.2% increase in peak strength when axial load was increased from 5% to 10%

Table 3. Comparison of the obtained displacement ductility capacity values

Model No.	Axial Load (kN)	Main Bar	Transverse Bar	μ_D Required	μ_D Obtained	Failure Mode
1	1358	14 (29M)	19M @ 76 mm	7.0	6.82	BF*
2	1358	14 (29M)	19M @ 76 mm	NA	6.13	BF
3	1358	14 (29M)	2 (19M) @ 76 mm	11.0	7.11	BF
4	1358	14 (29M)	2 (19M) @ 76 mm	NA	6.09	BF
5	2716	14 (29M)	19M @ 70 mm	7.0	7.27	BF
6	2716	14 (29M)	19M @ 70 mm	NA	5.62	CC**
7	2716	14 (29M)	2 (22M) @ 83 mm	11.0	7.28	BF
8	2716	14 (29M)	2 (22M) @ 83 mm	NA	6.27	BF
9	1358	14 (29M)	19M @ 76 mm	7.0	6.45	BF
10	1358	14 (29M)	19M @ 76 mm	NA	5.95	BF
11	1358	14 (29M)	2 (19M) @ 76 mm	11.0	6.47	BF
12	1358	14 (29M)	2 (19M) @ 76 mm	NA	5.90	BF
13	2716	14 (29M)	19M @ 70 mm	7.0	6.75	BF
14	2716	14 (29M)	19M @ 70 mm	NA	5.86	CC
15	2716	14 (29M)	2 (22M) @ 83 mm	11.0	6.67	BF
16	2716	14 (29M)	2 (22M) @ 83 mm	NA	6.12	BF
17	1358	20 (29M)	19M @ 64 mm	7.0	6.35	BF
18	1358	20 (29M)	19M @ 64 mm	NA	5.66	BF
19	1358	20 (29M)	2 (22M) @ 76 mm	11.0	6.37	BF
20	1358	20 (29M)	2 (22M) @ 76 mm	NA	5.61	BF
21	2716	20 (29M)	22M @ 76 mm	7.0	6.46	BF
22	2716	20 (29M)	22M @ 76 mm	NA	5.57	CC
23	2716	20 (29M)	2 (22M) @ 70 mm	11.0	6.54	BF
24	2716	20 (29M)	2 (22M) @ 70 mm	NA	5.73	BF
25	1358	20 (29M)	19M @ 64 mm	7.0	6.00	BF
26	1358	20 (29M)	19M @ 64 mm	NA	5.62	BF
27	1358	20 (29M)	2 (22M) @ 76 mm	11.0	5.94	BF
28	1358	20 (29M)	2 (22M) @ 76 mm	NA	5.60	BF
29	2716	20 (29M)	22M @ 76 mm	7.0	6.16	BF
30	2716	20 (29M)	22M @ 76 mm	NA	5.80	BF
31	2716	20 (29M)	2 (22M) @ 70 mm	11.0	6.10	BF
32	2716	20 (29M)	2 (22M) @ 70 mm	NA	5.65	BF

*Bar Fracture; **Core Crushing

ALI; this resulted in a larger stiffness for model 5. However, the displacement capacity is usually expected to decrease under larger axial loads as concrete crushing occurs earlier in the response. This phenomenon was not observed for model 5 because low-cycle fatigue bar fracture occurred before crushing of concrete. Figure 12b illustrates why low-cycle fatigue bar fracture for this particular column was rather insensitive to this level of change in axial load. The increased axial load affected the displacement capacity of models 6, 14, and 22; these were precast under 10% axial load and failed due to core concrete crushing, thus achieving a reduced ultimate displacement. Figure 12b shows the strain variation in the extreme longitudinal bars of models 1 and 5. Under larger axial load, there was an increase in compressive strains and a decrease in tensile strains for model 5, caused by a deeper neutral axis. Comparing the two curves, a strain shift occurred for model 5 under a larger axial load implying that the strain range, which is the main parameter in determining the low-cycle fatigue life of a reinforcing bar, remained similar to the one for model 1. This explains why model 5 did not fail before model 1.

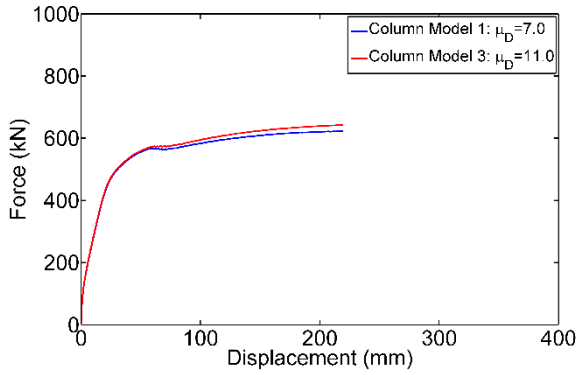

(a)

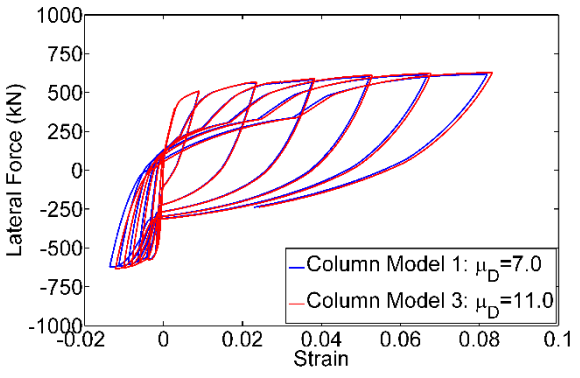

(b)

Figure 11. Effect of change in design displacement ductility for columns with (14) 29M bars

5.5 Effect of column height

The simulated columns had two clear heights of 3.66 m and 4.57 m corresponding to an aspect ratio equal to 4 and 5, respectively. An increase in column height (with identical sectional configurations) should result in a reduction in lateral force capacity since the moment arm becomes larger, as shown in the cyclic envelopes for models 1 and 9 in Figure 13a. Consequently, stiffness decreases resulting in a softer response for model 9. However, the displacement capacity of model 9 was found to be 45.8% larger than that of model 1 which is attributed to delayed bar fracture because of a lower demand on the critical section, as shown by the variation of strains for the extreme column bar of the two models (Figure 13b). Even though the displacement capacity of model 9 increased because of a larger height, the displacement ductility capacity decreased from 6.82 to 6.45, as discussed in the previous section. The reduction is due to the fact that the yield displacement also increases with an increase in column height (Figure 13a).

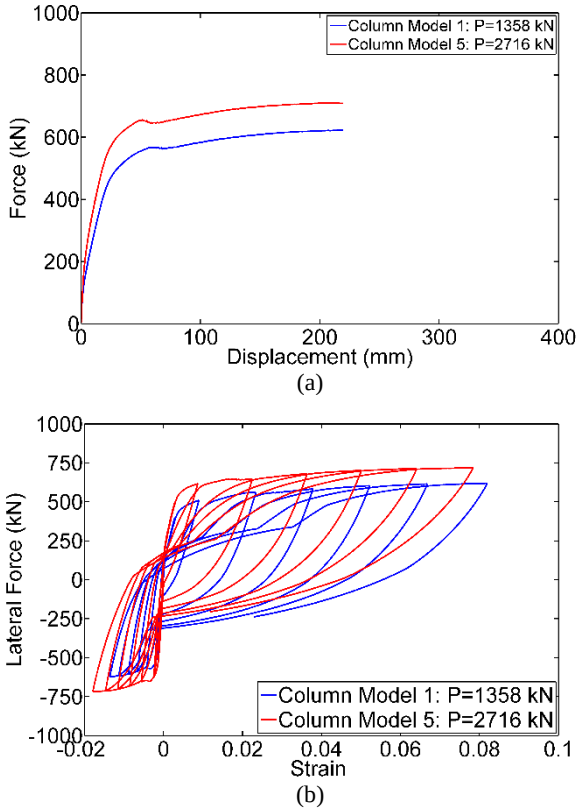

Figure 12. Effect of change in axial load for columns with (14) 29M bars

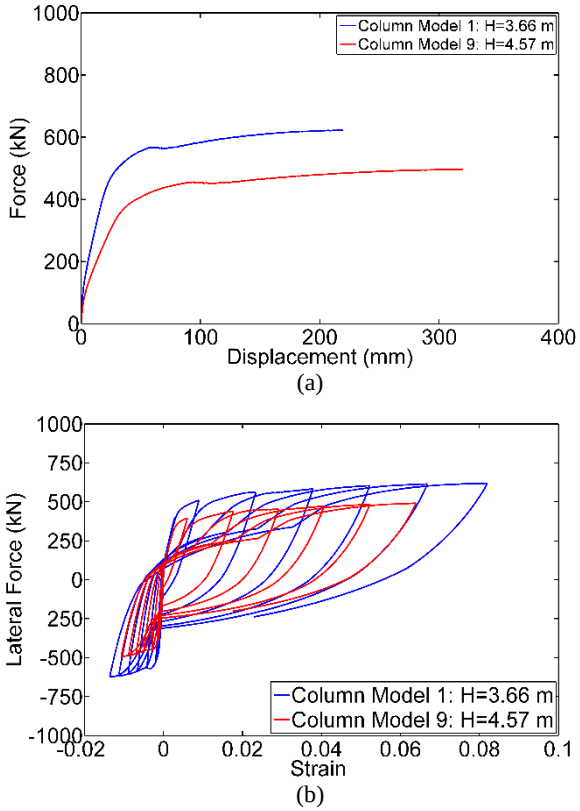

Figure 13. Effect of change in height for columns with (14) 29M bars

5.6 Effect of number of column longitudinal bars

Two longitudinal reinforcement ratios were considered equal to 1.38% and 1.96%, which correspond to fourteen and twenty 29M steel bars. A column reinforced with more longitudinal bars is expected to have a higher strength. The cyclic envelopes for model 1 and model 17 show that there was a 32.1% increase in the lateral force capacity when twenty 29M bars were used instead of fourteen 29M bars (Figure 14a). The post-cracking stiffness also increased by incorporating more longitudinal bars, as anticipated. The ultimate displacement, however, remained the same since both columns failed due to low-cycle fatigue bar fracture and the strain range in the column bars did not change significantly (Figure 14b). The strain variation indicates a small reduction of 2% in tensile strains for column model 17, followed by a slight increase in compressive strains implying a slightly deeper neutral axis which did not change the bar fracture drift ratio and cycle. The displacement ductility capacity was reduced from 6.82 for model 1 to 6.35 for model 17 because of a small increase in the effective yield displacement for model 17.

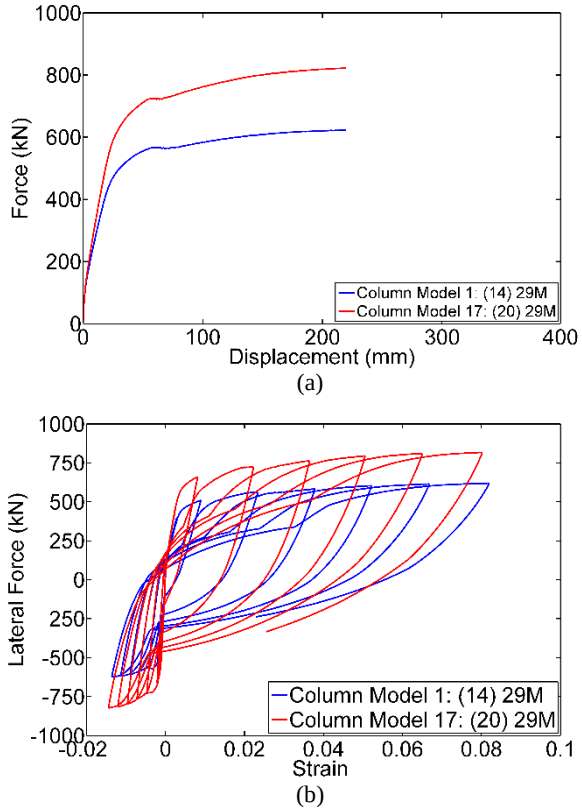

Figure 14. Effect of change in number of longitudinal bars

6 PLASTIC HINGE LENGTH VARIATION

Local response of columns is a function of the analytical plastic hinge length incorporated in the model. The design procedure discussed in Section 4.1 included recommendations regarding a reduced plastic hinge length for precast columns with GSS connectors. This section investigates the sensitivity in global and local responses of the Precast-2 column model when the plastic hinge length is varied using 13-mm length increments. The objective is to ascertain response sensitivity due to a change in the value of the reduced plastic hinge length. Precast column model 30 was selected which had twenty 29M longitudinal bars, a column height equal to 4.57 m, an ALI of 10%, and a design displacement ductility equal to 7.0. It was previously shown that the reduced plastic hinge length was 457 mm for this column model. An upper-bound and lower-bound plastic hinge length of 508 mm and 406 mm were used, respectively. Table 4 includes the response variation as a result of a change in the plastic hinge length. The failure mode was found to be either low-cycle fatigue bar fracture or crushing of core concrete. The column yield displacement

was unaffected while the sectional ultimate curvature, ultimate displacement, displacement ductility capacity, and mode of failure changed with a variation in the assumed plastic hinge length.

Table 4. Effect of plastic hinge length variation on sectional and global response of column model Precast-2

L_p (mm)	Failure Mode	ϕ_u @ 6% Drift (1/m)	Δ_y (mm)	Δ_u (mm)	μ_Δ
406	BF*	0.125	55.6	274.3	4.92
419	BF	0.122	55.6	274.3	4.93
432	CC**	0.119	55.6	312.7	5.61
445	BF	0.116	55.6	320.0	5.75
457***	BF	0.113	55.1	320.0	5.80
470	BF	0.111	55.4	320.0	5.77
483	BF	0.108	55.4	320.0	5.78
495	BF	0.106	55.4	320.0	5.79
508	BF	0.104	55.1	320.0	5.80

*Bar Fracture
**Core Crushing
***Plastic hinge length was equal to 457 mm based on proposed modeling strategy

The ultimate curvature at the 6% drift ratio changes as a result of varying plastic hinge length; sectional curvature increased with a decrease in the plastic hinge length (Figure 15a). The largest absolute curvature difference was found to be 10% for an 11% (51-mm) change in the plastic hinge length. Displacement ductility capacity decreased with a decrease in the plastic hinge length because of a larger sectional demand (Figure 15b). Displacement ductility capacity remained relatively unchanged at a value of 5.80 for an increase in the plastic hinge length from 457 mm to 508 mm because bar fracture due to low-cycle fatigue occurred at the 7% or 8% drift ratio for plastic hinge lengths equal to or greater than 457 mm. This resulted in an ultimate drift ratio equal to 7% (320 mm) for a plastic hinge length equal to or greater than 445 mm and smaller than 508 mm.

7 CONCLUSIONS

A parametric study was conducted on actual size bridge columns to assess the accuracy of the proposed modeling strategy for precast single-column bridge piers. The objective was to ascertain the applicability of the proposed model to both cast-in-place monolithic columns and precast bridge columns with grouted splice sleeve connectors. In addition, the effect of varying the parameters on

structural response was investigated. Two alternatives were considered: a cast-in-place column with monolithic details representing CIP elements, and a precast column with grouted splice sleeves in the column end and debonding of dowel

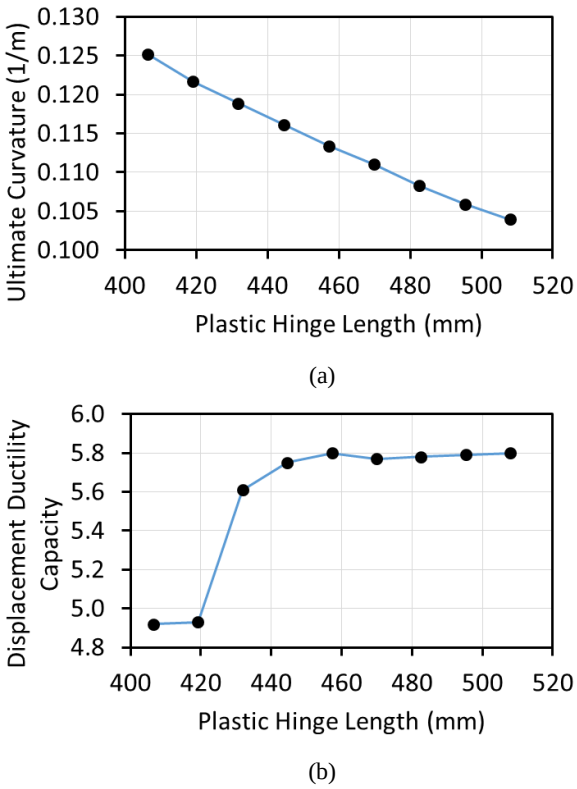

Figure 15. Effect of plastic hinge length variation on the response of Precast-2: (a) ultimate curvature during 6% drift ratio; (b) displacement ductility capacity

bars in the footing (Precast-2). Sixteen CIP and sixteen Precast-2 columns were examined with varying parameters. The findings of this parametric study apply to ductile slender columns investigated in this paper; extension of this modeling strategy to a more general group of columns with considerable design differences requires further investigation.

a) An empirical relationship was used to determine the length of the plastic hinge for cast-in-place column models. To include more localized damage for the precast column models, the computational model was constructed with a reduced plastic hinge length. In the absence of an empirical plastic hinge length relationship, a modeling strategy developed by the authors and outlined elsewhere was incorporated to account for premature bar fracture

due to localized higher strain levels as a result of using grouted splice sleeves at the column-to-footing interface.

b) All cast-in-place column models failed due to low-cycle fatigue bar facture, while precast column models failed due to low-cycle fatigue bar fracture and crushing of core concrete. The amount of axial load played an important role in the failure mode of precast column models.

c) The global strength of cast-in-place and precast models was similar for all models. Even though bar fracture occurred in fewer cycles for the precast alternatives, ultimate displacement was found to be identical to the cast-in-place models; this is because bar fracture occurred during the second cycle of the last drift ratio for the precast column models. That is, the displacement capacity of Precast-2 column models was close to that of CIP column models as was also observed in the experiments; however, displacement ductility of precast column models was found to be smaller than that of cast-in-place models due to a larger effective yield displacement, as a result of a larger bond-slip of the precast alternatives.

d) A large displacement ductility capacity is unachievable for bridge columns with modern seismic detailing under several displacement reversals due to low-cycle fatigue fracture of longitudinal bars. Even though a design displacement ductility of 11.0 was targeted for a number of column models, the maximum displacement ductility capacity in the simulations only reached 7.28.

e) An increase in the design displacement ductility resulted in increased confined concrete properties in terms of both stress and strain. Consequently, there was a small increase in the lateral force capacity of the column model; however, displacement capacity was unaffected since bar fracture occurred before crushing of the core concrete. Greater confinement was found to have a small effect on the low-cycle fatigue life of the column bars.

f) Column lateral strength increased with an increase in the column axial load for models with design capacities below the balanced point. The displacement capacity of three column models was reduced because of increased compressive demand which resulted in crushing of the core concrete. The displacement capacity of the remaining 29 column models was not affected by an axial load increase because there was a considerable remaining compressive strain capacity when bar fracture due to low-cycle fatigue bar occurred.

g) An increase in column height resulted in a decrease in lateral strength. Displacement capacity increased with an increase in column model height because of a lower strain demand at the column end. However, the displacement ductility capacity did not increase because the effective yield displacement of the taller column model was larger than that of the shorter column model.

h) Column models reinforced with a larger number of longitudinal bars had a higher lateral strength; the displacement capacity was not affected since sectional strain demand did not change drastically. Thus, low-cycle fatigue life of column models with a large number of longitudinal bars was similar to that of column models with fewer bars.

REFERENCES

[1] Khaleghi, B, Schultz, E, Seguirant, S, Marsh, L, Haraldsson, OS, Eberhard, MO, Stanton, JF, "Accelerated Bridge Construction in Washington State: From Research to Practice", PCI Journal, Vol. 57, No. 4, pp. 34–49, 2012.

[2] Weinert, MD, "Substructure Connections for Accelerated Bridge Construction in Seismic Regions", MS Thesis, University of Washington, Seattle, WA, 2011.

[3] Haraldsson, OS, Janes, TM, Eberhard, MO, Stanton, JF, "Seismic Resistance of Socket Connection between Footing and Precast Column", Journal of Bridge Engineering, Vol. 18, No. 9, pp. 910–919, 2013.

[4] Belleri, A, Riva, P, "Seismic Performance and Retrofit of Precast Concrete Grouted Sleeve Connections", PCI Journal, Vol. 57, No. 1, pp. 97–109, 2012.

[5] White, S, "Controlled Damage Rocking Systems for Accelerated Bridge Construction", MS Thesis, University of Canterbury, Christchurch, New Zealand, 2014.

[6] Matsumoto, EE, "Emulative Precast Bent Cap Connections for Seismic Regions: Component Tests-Grouted Duct Specimen (Unit 2)", *ECS Report No. ECS-CSUS-2009-02*, California State University, Sacramento, CA, 2009.

[7] Pang, JBK, Eberhard, MO, Stanton, JF, "Large-bar Connection for Precast Bridge Bents in Seismic Regions", Journal of Bridge Engineering, Vol. 15, No. 3, pp. 231–239, 2010.

[8] Tazarv, M, Saiidi, MS, "UHPC-filled Duct Connections for Accelerated Bridge Construction of RC Columns in High Seismic Zones", Engineering Structures, Vol. 99, pp. 413–422, 2015.

[9] Marsh, ML, Wernly, M, Garett, BE, Stanton, JF, Eberhard, MO, Weinert, MD, "Application of Accelerated Bridge Construction Connections in Moderate-to-high Seismic Regions", *NCHRP Report 698*, National Cooperative Highway Research Program, Washington, DC, 2011.

[10] Jansson, PO, "Evaluation of Grout-filled Mechanical Splices for Precast Concrete Construction", *Report R-1512*, Michigan Department of Transportation, Lansing, MI, 2008.

[11] Rowell, SP, Grey, CE, Woodson, SC, Hager, KP, "High Strain Rate Testing of Mechanical Couplers", *Report ERDC TR-09-8*, Washington, DC, 2009.

[12] Haber, ZB, Saiidi, MS, Sanders, DH, "Behavior and Simplified Modeling of Mechanical Reinforcing Bar Splices", ACI Structural Journal, Vol. 112, No. 2, pp. 179-188, 2015.

[13] Ameli, MJ, Parks, JE, Brown, DN, Pantelides, CP, "Seismic Evaluation of Grouted Splice Sleeve Connections for Reinforced Precast Concrete Column-to-cap beam Joints in Accelerated Bridge Construction", PCI Journal, Vol. 60, No. 2, pp. 80-103, 2015.

[14] Tazarv, M, Saiidi, MS, "Next Generation of Bridge Columns for Accelerated Bridge Construction in High Seismic Zones", *Report CCEER14-06*, Center for Civil Engineering Earthquake Research, Department of Civil and Environmental Engineering, University of Nevada-Reno, Reno, NV, 2014.

[15] Haber, ZB, Saiidi, MS, Sanders, DH, "Seismic Performance of Precast Columns with Mechanically Spliced Column-footing Connections", ACI Structural Journal, Vol. 111, No. 3, pp. 639-650, 2014.

[16] Aida, H, Tanimura, Y, Tadokoro, T, Takimoto, K, "Cyclic Loading Experiment of Precast Columns of Railway Rigid-frame Viaduct Installed with NMB Splice Sleeves", *Proc. Japan Concrete Institute*, Vol. 27, No. 2, 2005.

[17] Reetz, RJ, Ramin, MV, Matamoros, A, "Performance of Mechanical Splices within the

Plastic Hinge Region of Beams Subject to Cyclic Loading", *Proceedings of 13th World Conference on Earthquake Engineering*, Vancouver, B.C., Canada, 2004.
[18] Yoshino, T., Kobayashi, K., Ase, M, "Intensive shear reinforcing method for PCA members with splice sleeve joint", *Proc. 11th World Conference on Earthquake Engineering*, Acapulco, Mexico, 1996.
[19] Matsuzaki, Y, et al., "Effects of Sleeves on Member Properties: Study on the Behavior of Reinforced Concrete Beams with Grout-filled Steel Splice Sleeves", Architectural Institute of Japan, 1987.
[20] Splice Sleeve Japan, Ltd. (unpublished), "Tests on Re-bar Splices in Reinforced Concrete Columns using NMB Splice Sleeves", *Report NPD-024*, Splice Sleeve Japan, Ltd., Tokyo, Japan.
[21] Ameli, MJ, Brown, DN, Parks, JE, Pantelides, CP, "Seismic Column-to-footing Connections using Grouted Splice Sleeves", ACI Structural Journal, Vol. 113, No. 5, pp. 639-650, 2016.
[22] Ameli, MJ, Pantelides, CP, "Seismic Analysis of Precast Concrete Bridge Columns Connected with Grouted Splice Sleeve Connectors", Journal of Structural Engineering, 04016176, 2016.
[23] AASHTO, *AASHTO Guide Specifications for LRFD Seismic Bridge Design*, Washington, DC, 2011.
[24] AASHTO, *AASHTO LRFD Bridge Design Specification*, Washington, DC, 2012.
[25] California Department of Transportation, *Caltrans Seismic Design Criteria*, Version 1.7, http://www.dot.ca.gov/hq/esc/earthquake_engineering/sdc/documents/Seismic-Design-Criteria-(SDC-1.7-Full-Version,-OEE-Release).pdf, 2013.
[26] Scott, M. and Fenves, G. "Plastic Hinge Integration Methods for Force-Based Beam–Column Elements", Journal of Structural Engineering, 10.1061/(ASCE)0733-9445(2006)132:2(244), 244–252, 2006.
[27] Kunnath, S., Heo, Y., and Mohle, J. "Nonlinear uniaxial material model for reinforcing steel bars." Journal of Structural Engineering, 10.1061/(ASCE)0733-9445(2009)135:4(335), 335–343, 2009.
[28] Priestley, MJN, Seible, F, Calvi, GM, *Seismic Design and Retrofit of Bridges*, John Wiley and Sons, Inc., New York, NY, 1996.
[29] Panagiotakos, TB, Fardis, MN, "Deformations of Reinforced Concrete Members at Yielding and Ultimate", ACI Structural Journal, Vol. 98, No. 2, pp. 135–148, 2001.
[30] Mander, JB, Priestley, MJN, Park, R, "Theoretical Stress-strain Model for Confined Concrete", Journal of Structural Engineering, 10.1061/(ASCE)0733-9445(1988)114:8(1804), 1804-1826, 1988.
[31] McKenna, F, Fenves, G, Scott, M, "Open System for Earthquake Engineering Simulation (OpenSees)", Univ. of California, Berkeley, CA, (*http://opensees.berkeley.edu*), 2000.
[32] Ameli, MJ, "Seismic Evaluation of Grouted Splice Sleeve Connections for Bridge Piers in Accelerated Bridge Construction", PhD Dissertation, Univ. of Utah, Salt Lake City, UT, 2016.
[33] American Concrete Institute (ACI) Committee 374, "Guide for Testing Reinforced Concrete Structural Elements under Slowly Applied Simulated Seismic Loads", *ACI 374*, Farmington Hills, MI, 2013.